Arg-8 of yeast subunit e contributes to the stability of F-ATP synthase dimers and to the generation of the full-conductance mitochondrial megachannel

Received for publication, April 11, 2019, and in revised form, May 29, 2019 Published, Papers in Press, June 3, 2019, DOI 10.1074/jbc.RA119.008775

Lishu Guo[‡1], Michela Carraro[‡], Andrea Carrer[‡], Giovanni Minervini[‡], Andrea Urbani[‡], Ionica Masgras[‡], Silvio C. E. Tosatto[‡§], Ildikò Szabò[§¶], Paolo Bernardi[‡§2], and Giovanna Lippe[‖3]

From the Departments of [‡]Biomedical Sciences and [¶]Biology, University of Padova, 35131 Padova, Italy, the [§]Consiglio Nazionale delle Ricerche Institute of Neuroscience, 35131 Padova, Italy, and the [‖]Department of Agricultural, Food, Environmental and Animal Sciences, University of Udine, 33100 Udine, Italy

Edited by John M. Denu

The mitochondrial F-ATP synthase is a complex molecular motor arranged in V-shaped dimers that is responsible for most cellular ATP synthesis in aerobic conditions. In the yeast F-ATP synthase, subunits e and g of the F_O sector constitute a lateral domain, which is required for dimer stability and cristae formation. Here, by using site-directed mutagenesis, we identified Arg-8 of subunit e as a critical residue in mediating interactions between subunits e and g, most likely through an interaction with Glu-83 of subunit g. Consistent with this hypothesis, (i) the substitution of Arg-8 in subunit e (eArg-8) with Ala or Glu or of Glu-83 in subunit g (gGlu-83) with Ala or Lys destabilized the digitonin-extracted F-ATP synthase, resulting in decreased dimer formation as revealed by blue-native electrophoresis; and (ii) simultaneous substitution of eArg-8 with Glu and of gGlu-83 with Lys rescued digitonin-stable F-ATP synthase dimers. When tested in lipid bilayers for generation of Ca^{2+}-dependent channels, WT dimers displayed the high-conductance channel activity expected for the mitochondrial megachannel/permeability transition pore, whereas dimers obtained at low digitonin concentrations from the Arg-8 variants displayed currents of strikingly small conductance. Remarkably, double replacement of eArg-8 with Glu and of gGlu-83 with Lys restored high-conductance channels indistinguishable from those seen in WT enzymes. These findings suggest that the interaction of subunit e with subunit g is important for generation of the full-conductance megachannel from F-ATP synthase.

The mitochondrial F-ATP synthase is a molecular rotary motor that uses the protonmotive force existing across the inner membrane of the organelle to make ATP from ADP and phosphate. The enzyme is a multisubunit complex with a mass of about 600 kDa, composed of a soluble F_1 sector that functions as the catalytic core and a membrane-embedded F_O sector linked to F_1 by central and peripheral stalks (1). The F_1 moiety consists of five subunits denoted as α, β, γ, δ, and ϵ with a 3:3:1:1:1 stoichiometry (2). Subunits α and β are organized into an $\alpha_3\beta_3$ hexamer, and subunit γ is located inside the $\alpha_3\beta_3$ subcomplex (3). Subunit γ interacts with subunits δ and ϵ at the foot of the central stalk contacting the c-ring, which in yeast comprises 10 c subunits (4). These are all key elements of the rotor that couples the protonmotive force to the synthesis of ATP. Proton translocation through two offset half-channels in the F_O region, located at the interface of the c-ring and subunit a (5), drives rotation of the central rotor that induces conformational changes within the $\alpha_3\beta_3$ sub-complex leading to the synthesis of ATP (1). The co-rotation of α and β subunits with γ is prevented by the peripheral stalk, which is formed by the subunits oligomycin sensitivity conferral protein (OSCP),[4] d and h (F_6 in mammals), the soluble region of subunit b (1, 6, 7), and by the subunits 8 (A6L in mammals) (8) and f (8) in the lower part as it leaves the inner membrane.

Besides the already mentioned subunits, the yeast complex consists of five additional subunits located in the membrane-embedded part of F_O (e, g, i/j, k, and l) that are not essential for its assembly and catalysis, the so-called "supernumerary subunits." A recent electron cryo-microscopy map of the yeast enzyme has shown that subunits e and g and the N-terminal ~50 residues of subunit b, with the further support from subunit k, shape a lateral domain responsible for bending the inner membrane (8). These bends drive self-assembly of F-ATP synthase monomers into V-shaped dimers, which then oligomerize to form long ribbons giving rise to the characteristic mitochondrial cristae (9–11). Indeed, pioneering studies had demonstrated that ablation of either subunits e or g leads to disappearance of the dimers extracted with digitonin and separated by blue native-gel electrophoresis (BN-PAGE) as well as

This work was supported in part by AIRC Grant IG17067 (to P. B.) and Fondation Leducq Grant 16CVD04 (to P. B.). This work is in partial fulfillment of the requirements for the Ph.D. at the Department of Biomedical Sciences, University of Padova (L. G.). The authors declare that they have no conflicts of interest with the contents of this article.

This article contains Figs. S1–S5.

[1] Supported by a fellowship from the China Scholarship Council.

[2] To whom correspondence may be addressed: Dept. of Biomedical Sciences, University of Padova, 35131 Padova, Italy. Tel. 39-049-8276365; Fax: 39-049-827-6049; E-mail: bernardi@bio.unipd.it.

[3] To whom correspondence may be addressed. Tel.: 39-0432-558139; Fax: 39-0432-558130; E-mail: giovanna.lippe@uniud.it.

[4] The abbreviations used are: OSCP, oligomycin sensitivity conferral protein; MMC, mitochondrial megachannel; PTP, permeability transition pore; BN-PAGE, blue native-PAGE; BisTris, 2-bis(2-hydroxyethyl)amino-2-(hydroxymethyl)-1,3-propanediol; DKO, double knockout Δ*TIM11*Δ*ATP20* mutant; ANOVA, analysis of variance; PVDF, polyvinylidene difluoride; Tricine, *N*-[2-hydroxy-1,1-bis(hydroxymethyl)ethyl]glycine; CN-PAGE, clear native-PAGE; pF, picofarad.

to formation of an onion-like ultrastructure of mitochondria (12–14). The cryo-EM map has also established that the dimer interface within the inner membrane (i) is formed by subunits i/j and by two strands of subunit a from each monomer and (ii) is stabilized by the interactions with subunits e and k (8). Because cross-linking analysis has placed the N terminus of subunit b next to subunit g, it has been proposed that subunit b interacts with subunit g, which contacts subunit e favoring enzyme dimerization (15, 16).

In addition to mediating cristae formation, F-ATP synthase has been proposed to generate the mitochondrial permeability transition pore (PTP), also called mitochondrial megachannel (MMC), an unselective high-conductance channel that can trigger cell death as a consequence of long-lasting openings (17–20). Indeed, partially purified F-ATP synthase from bovine hearts (17), mammalian cells (21), *Saccharomyces cerevisiae* (22), and *Drosophila melanogaster* (23) displayed channel activity that was close to that expected for the native MMC/PTP. We have hypothesized that conformational changes induced by Ca^{2+} binding to the catalytic core of F-ATP synthase (24) are transmitted through OSCP and the lateral stalk (19, 24) causing an opening of a channel within F_O, possibly where subunits e and g and the N terminus of subunit b are located (8, 22). Remarkably, ablation of subunits e and g leads to the disappearance of the high-conductance MMC/PTP (25) like ablation of subunit c (26), which prevents enzyme assembly (27); and recent work suggests that Arg-107 of subunit g (which is located at the C terminus) may contribute to formation of the yeast channel (28). A peculiar feature of the yeast enzyme is that both e and g subunits possess a conserved G*XXX*G motif located in their unique transmembrane domain that appears to be involved in their interaction (29–31). This study aimed at testing whether charged amino acids are also involved in the association of the dimer-specific subunits e and g in yeast and at assessing whether the subunit e/g interface plays a role in MMC/PTP activity.

Results

Substitution of Arg-8 in subunit e affects stability of F-ATP synthase dimers

Arg-8 of subunit e (eArg-8), encoded by the yeast *TIM11* gene, is the only arginine conserved across species (Fig. S1*A*). We substituted eArg-8 with either Ala or Glu in *S. cerevisiae* strain BY4743 using site-directed mutagenesis. These two subunit e variants were expressed in the Δ*TIM11* mutant lacking subunit e. As a control, we also re-expressed the WT subunit e in the Δ*TIM11* mutant (TIM11 WT). Mitochondrial proteins from TIM11 R8A and R8E mutants were extracted with increasing digitonin concentrations and compared with those from Δ*TIM11* and TIM11 WT strains, as well as to those from the mutant strain lacking subunit g (Δ*ATP20*). BN-PAGE followed by Coomassie Blue staining and in-gel ATPase activity assays revealed that, as expected, the Δ*TIM11* and Δ*ATP20* mutants displayed only monomers irrespective of the digitonin–to–protein ratios, whereas in the BY4743 and TIM11 WT strains dimers were readily detectable along with monomers at all digitonin concentrations. In contrast, in the extracts from TIM11 R8A and R8E mutants, dimers were present at low but not at higher digitonin–to–protein ratios (Fig. 1*A* and Fig. S2, *A–D*). Comparison of the dimer/monomer ratios of the different genotypes demonstrates that in the TIM11 R8A and R8E mutants the presence of dimers was dramatically decreased (Fig. 1*B*). In the TIM11 R8A and R8E mutants the expression levels of subunits e and g relative to subunit b were similar to those of the TIM11 WT strain both in whole-cell and mitochondrial lysates (Fig. 1, *C* and *D*). Consistent with an earlier study (12), in the Δ*TIM11* mutant subunit g was not detected, whereas in the Δ*ATP20* mutant lacking subunit g cellular and mitochondrial steady-state levels of subunit e were slightly decreased compared with the BY4743 strain (Fig. 1*C*). The generation times of TIM11 R8A and TIM11 R8E mutants cultured in the selective respiratory liquid medium (Drop-out–uracil containing 1% v/v ethanol and 1% v/v glycerol) were not significantly different from those of the BY4743 and TIM11 WT strains (Fig. S3*A*). Also, respiratory rates and respiratory control ratios of the TIM11 R8A and R8E mutants were comparable with those of TIM11 WT mitochondria (Fig. S3*B*). Somewhat surprisingly, the TIM11 R8A and R8E mutants also displayed a normal mitochondrial morphology, which was indistinguishable from that of the TIM11 WT or BY4743 strains (Fig. S4). In contrast, and as expected based on previous work (13, 14), in the Δ*TIM11* the mutant cristae morphology was markedly affected, with the presence of the typical onion-like structures. These findings suggest that the TIM11 R8A and R8E mutations do not cause major effects on F-ATP synthase assembly, but they do cause an increased tendency of the dimers to dissociate when extracted with digitonin and run in BN-polyacrylamide gels.

Substitution of Arg-8 affects incorporation of subunit e in the F-ATP synthase dimers

$CuCl_2$ treatment leads to F-ATP synthase dimer formation even in mutants lacking subunit e (Δ*TIM11*) or subunit g (Δ*ATP20*) through copper-induced formation of disulfide bridges that can be easily detected by BN-PAGE (22, 25, 30). After cross-linking with copper, dimer/monomer ratios similar to those of the WT genotypes were observed in Δ*TIM11*, Δ*ATP20*, TIM11 R8A, and TIM11 R8E mutants (Fig. 2*A*). To assess the relative abundance of subunit e after $CuCl_2$ treatment, the BN gels were transferred to PVDF membranes and immunoblotted for subunit b or e. The levels of subunit b were consistent with the protein abundance detected in BN gels, and as expected, subunit e was present in the dimers of WT BY4743 and TIM11 WT strains and absent in the Δ*TIM11* mutant (Fig. 2*B*). Remarkably, deletion of subunit g prevented accommodation of subunit e within F-ATP synthase dimers; indeed, subunit e was almost exclusively associated with the monomers despite the enforced dimerization induced by copper (Fig. 2*B*). A similar, albeit smaller, effect was caused by the TIM11 R8A and R8E mutations in subunit e, where a fraction of the protein was found in the monomers (Fig. 2*B*). This is a novel finding suggesting that each of these point mutations decreases the strength of interaction between subunits e and g and therefore dimer stability.

We also analyzed extracts of mitochondria not treated with copper by clear native gel electrophoresis (CN-PAGE), followed by immunoblotting. CN-PAGE is milder than BN-PAGE

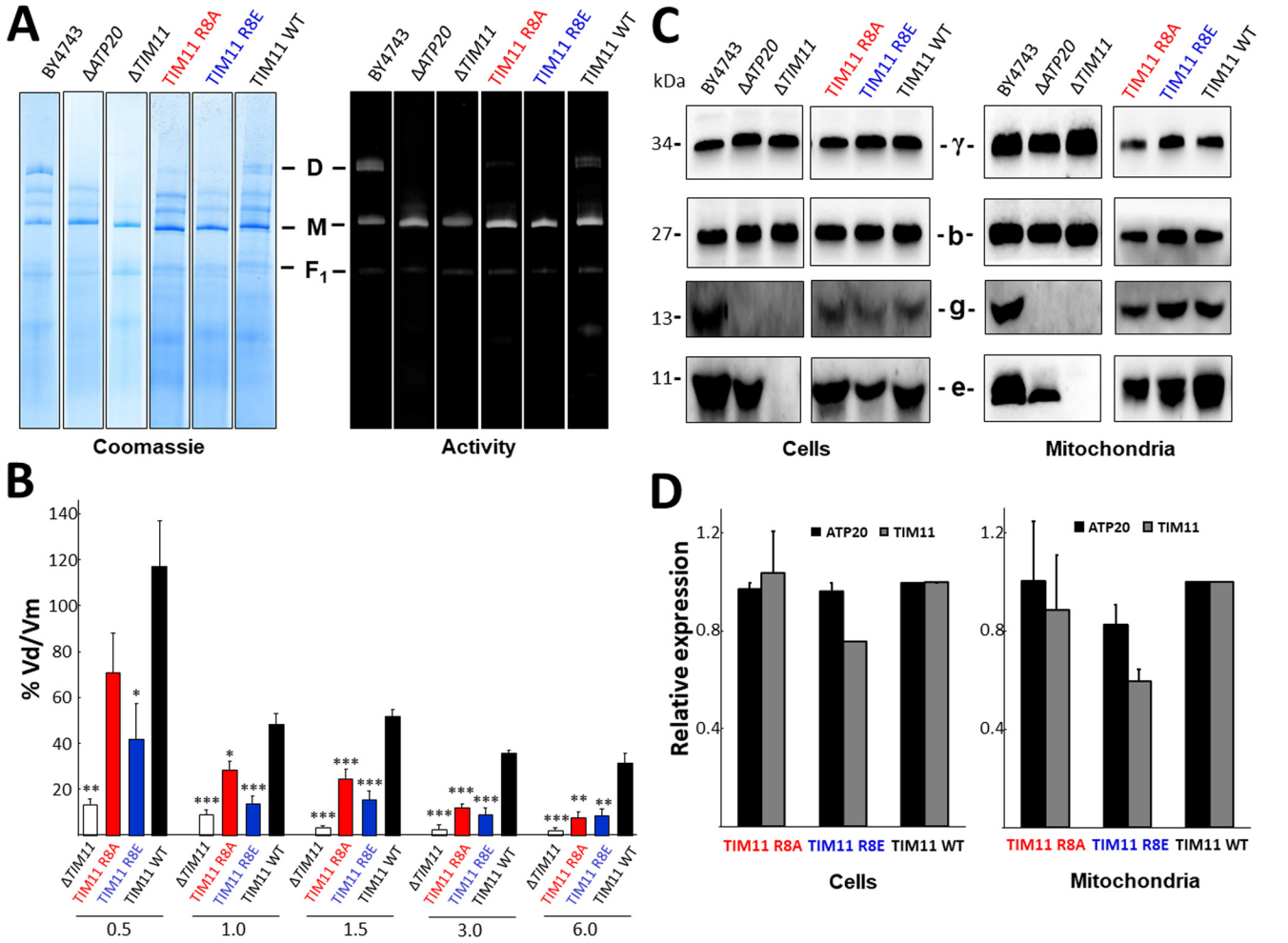

Figure 1. Substitutions of Arg-8 of yeast subunit e affect F-ATP synthase dimer stability. *A,* mitochondria with the indicated genotypes were solubilized with a digitonin–to–protein ratio of 1.5 g/g and centrifuged, and the protein extracts were subjected to BN-PAGE to separate the dimers, monomers, and F_1 sector of F-ATP synthase identified by Coomassie Blue and in-gel activity staining. Monomers and dimers are denoted as *M* and *D*, respectively. The figures are representative of at least three independent experiments. *B,* histograms report the abundance of dimers relative to that of monomers (taken as 100%) and were obtained by densitometric analysis of BN gels stained for in-gel activity. The indicated digitonin–to–protein ratios (g/g) were used for mitochondria solubilization. Data are an average ± S.E. of at least three independent experiments. *, $p < 0.05$ *versus* TIM11WT; **, $p < 0.01$ *versus* TIM11WT; ***, $p < 0.001$ *versus* TIM11WT. One-way ANOVA was used for statistical analysis. *C,* total cell lysate or mitochondrial proteins from indicated genotypes were separated by SDS-PAGE and analyzed by Western blotting. The figures are representative of at least three independent experiments. *D,* histograms represent the relative densitometry values of TIM11 or ATP20 relative to subunit b and normalized to TIM11 WT. Data are presented as mean ± S.E. of at least three independent experiments.

because the dimeric structures of F-ATP synthase are better preserved in the absence of the anionic Coomassie dye (32–34) as shown even in yeast mutants lacking subunit e or g (34). Dimers were clearly identified in all strains, including the Δ*TIM11* and Δ*ATP20* mutants (Fig. 2*C*). However, and consistent with the results of the BN-PAGE analysis in Fig. 1*A*, substitution of eArg-8 in the TIM11 R8A and R8E mutants decreased the abundance of dimers, especially at higher digitonin (Fig. 2*C*). Also in these protocols, subunit e was not detected in the dimers of the Δ*ATP20* mutant lacking subunit g, and a small fraction of subunit e was associated with F-ATP synthase monomers in the TIM11 R8A and R8E mutants (Fig. 2*D*).

Glu-83 of subunit g interacts with Arg-8 of subunit e

Subunit g possesses two Glu residues, the only two negatively charged amino acids conserved in this subunit (Fig. S1*B*). To investigate whether they interact with Arg-8 of subunit e, we generated alanine and lysine mutants at Glu-83 and Glu-102 (which is located within the G*XXX*G motif) of subunit g. The four mutated and WT subunits g were re-expressed in the Δ*ATP20* mutant (lacking subunit g), and the digitonin extracts of mitochondria were analyzed by BN-PAGE. As expected, the Δ*ATP20* mutant displayed only monomers, whereas in the BY4743 and ATP20 WT strains dimers were clearly detectable along with monomers (Fig. 3, *A* and *B*). Interestingly, the dimer/monomer ratios of the ATP20 E83A and ATP20 E83K mutants were significantly decreased, whereas the ATP20 R102A or ATP20 R102K mutation had no effect (Fig. 3, *A* and *B*). The expression levels of subunits e and g were unaffected by these mutations (Fig. S5). Thus, the significant reduction of dimeric complexes in the ATP20 E83A and E83K mutants cannot be explained by reduced steady-state levels of the mutated subunit g. Remarkably, the combination of an R8E mutation in subunit e with an E83K mutation in subunit g was able to rescue dimer formation, which was detectable in BN gels, similar to the re-expression of TIM11 and ATP20 WT (Fig. 3*C*). The

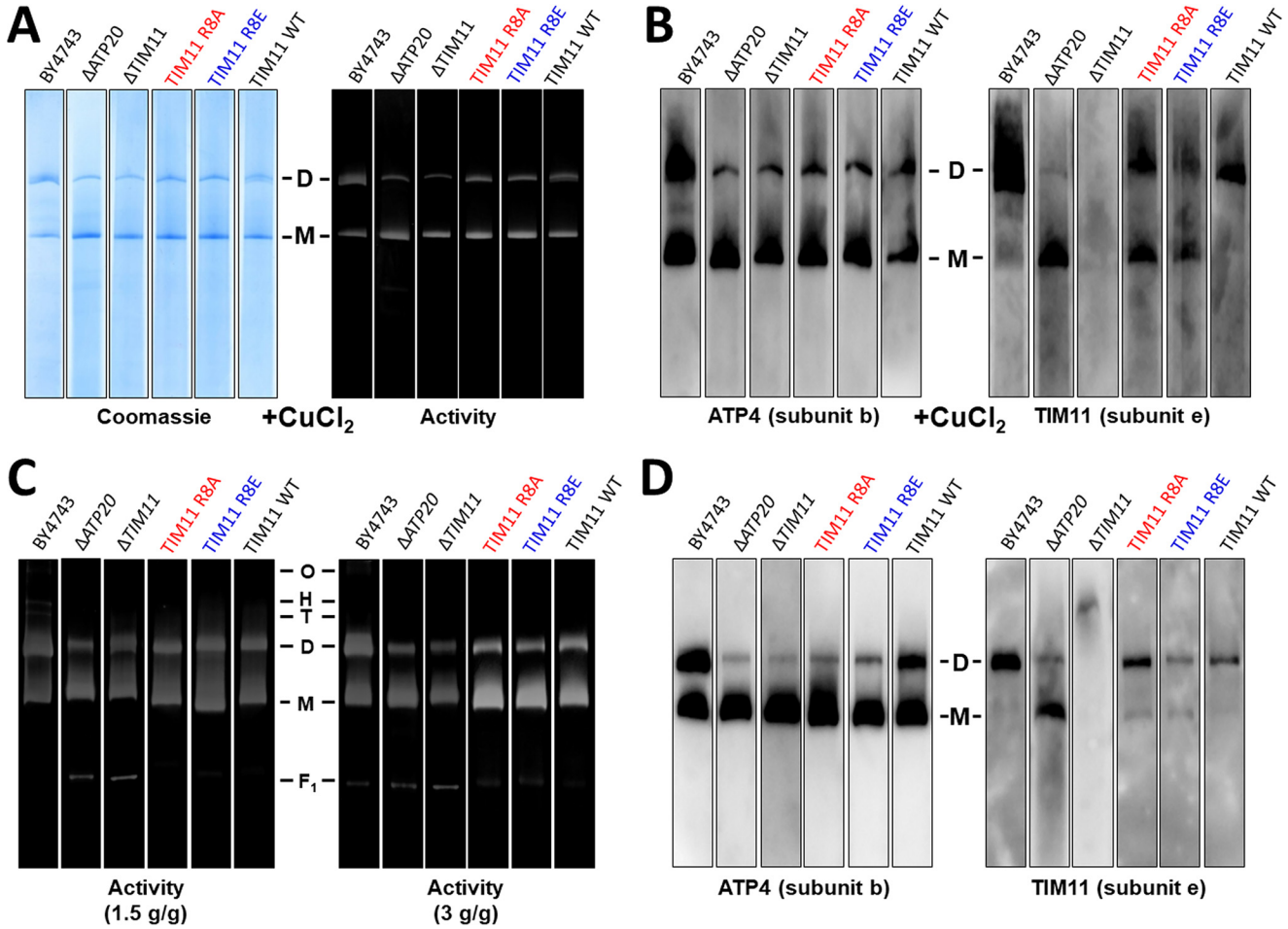

Figure 2. Substitution of Arg-8 affects the stable incorporation of subunit e in F-ATP synthase dimers. *A,* after pretreatment with $CuCl_2$ as described under "Experimental procedures," protein extracts (obtained with a digitonin–to–protein ratio of 1.5 g/g) from mitochondria with the indicated genotypes were separated by BN-PAGE and stained with Coomassie Blue or identified by in-gel activity staining. *B,* BN gels as described in *A* were subjected to immunoblotting for subunit b or e. Monomers and dimers are denoted as *M* and *D*, respectively. *C,* mitochondrial proteins from strains of the indicated genotypes were extracted with the indicated digitonin–to–protein ratios and separated by CN-PAGE and subjected to in-gel activity staining. *D,* CN gels of protein extracts obtained with a digitonin–to–protein ratio of 1.5 g/g were subjected to immunoblotting for subunit b or e. Monomers and dimers are denoted as *M* and *D*, respectively. All the figures are representative of at least three independent experiments.

Δ*TIM11*Δ*ATP20* mutant had a significantly longer generation time than the BY4743 strain (Fig. S3*A*). Ablation of *TIM11* and *ATP20* followed by re-expression of TIM11 R8E and ATP20 E83K did not significantly affect growth and respiratory properties of the mutants, which came close to those of the strain re-expressing WT TIM11 + ATP20 (Fig. S3, *A* and *C*). These data indicate that Glu-83 of subunit g participates in the interaction with Arg-8 of subunit e thus favoring dimer stability.

A couple of charged residues at position 8 in subunit e and at position 83 in subunit g is required for generation of the full-conductance megachannel

Based on the possible role of subunit e in formation of a Ca^{2+}-dependent, MMC/PTP-like channel by F-ATP synthase (22, 25), we assessed the channel properties of the TIM11 R8A and R8E mutant dimers after extraction at a low digitonin–to–protein ratio (*i.e.* in the absence of copper). Dimers cut out from BN gels were eluted and reconstituted into planar lipid bilayers, followed by detection of their electrophysiological properties. Compared with the dimers from TIM11 WT mitochondria, which showed the high-conductance openings expected for the native channel, dimers from the TIM11 R8A and R8E mutants displayed strikingly smaller channel activities, with a marked decrease of both the relative $|P(f)|$ area (curve under the power spectrum) and of the mean currents (Fig. 4). In all strains, channel activity was completely blocked by 1 mM Gd^{3+}, an inhibitor of the MMC/PTP (25). Interestingly, in the TIM11 R8E mutant the maximal current (but no other features of the currents) was similar to that of the TIM11 WT. A possible explanation is that in the R8E mutant Glu-8 forms transient interactions with Lys-81 or Lys-86 of subunit g, two nonconserved positive residues present only in *S. cerevisiae*. To further investigate the role of subunit e/g interactions in generation of the full-conductance MMC/PTP, we also tested the channel activity of the eGlu-8 and gLys-83 double mutants. Remarkably, this mutant displayed channel properties indistinguishable from those of the WT enzyme (Fig. 4).

The substitution of gArg-107 with Ala prevents the inhibitory effect of phenylglyoxal on the PTP and slows down solute permeation (28). We therefore also tested the consequences of the R107A and R107E mutations, which both led to a marked decrease of the Ca^{2+}-dependent currents across the MMC/

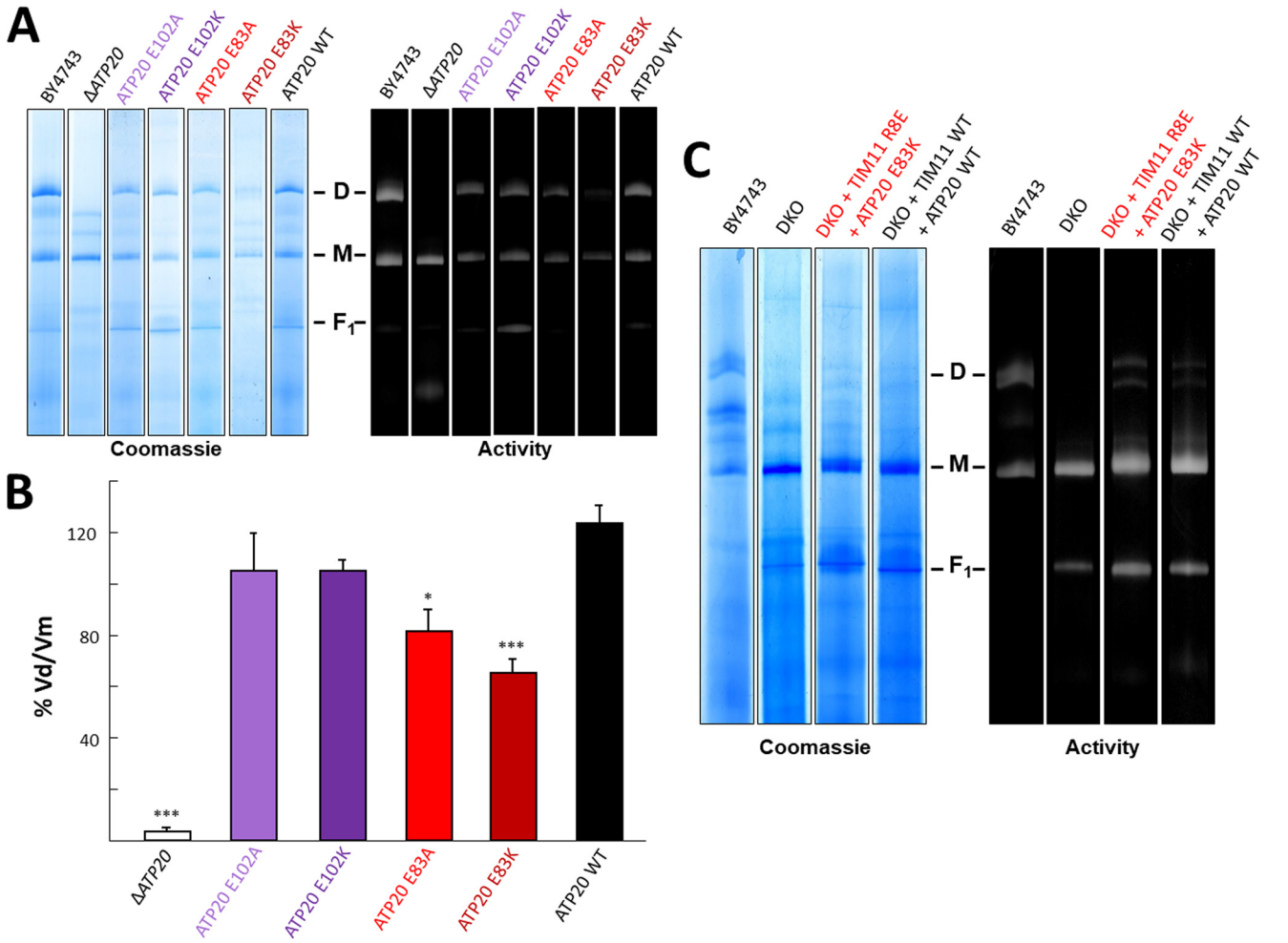

Figure 3. Glu-83 of subunit g interacts with Arg-8 of subunit e favoring F-ATP synthase dimer stability. *A,* protein extracts (obtained with a digitonin–to–protein ratio of 1.5 g/g) from mitochondria of the indicated genotypes were subjected to BN-PAGE to separate dimers, monomers, and the F_1 sector of F-ATP synthase identified by Coomassie Blue and in-gel activity staining. Monomers and dimers are denoted as *M* and *D*, respectively. Gels are representative of at least three independent experiments. *B, histograms* report the abundance of dimers relative to that of monomers (taken as 100%) and were calculated by densitometric analysis of the in-gel activity-stained BN gels relative to extracts obtained with 1.5 g/g (digitonin/protein) from mitochondria with the indicated genotypes. Data are presented as mean ± S.E. of at least three independent experiments. *, $p < 0.05$ *versus* ATP20WT; ***, $p < 0.001$ *versus* ATP20WT. One-way ANOVA was used for statistical analysis. *C,* protein extracts with 1.5 g/g (digitonin/protein) from mitochondria of the indicated genotypes were subjected to BN-PAGE, and dimers, monomers, and F_1 sector of F-ATP synthase were identified by Coomassie Blue staining and in-gel activity staining. Monomers and dimers are denoted as *M* and *D*, respectively. *Lanes from left to right* represent the genotypes BY4743, Δ*TIM11*Δ*ATP20* mutant (DKO), Δ*TIM11*Δ*ATP20* mutant re-expressing TIM11 R8E, and ATP20 E83K (DKO + TIM11 R8E + ATP20 E83K), Δ*TIM11*Δ*ATP20* mutant re-expressing TIM11 WT and ATP20 WT (DKO + TIM11 WT + ATP20 WT) as indicated, respectively. The panels report one representative experiment of at least three independent replicates.

PTP, which maintained full sensitivity to inhibition by Gd^{3+} (Fig. 5).

Taken together, these results indicate the region where the PTP forms involves subunits e/g and their interface.

Discussion

Digitonin is widely used to isolate membrane multiprotein complexes and allows separation of various forms of F-ATP synthase as a function of the digitonin–to–protein ratios used, *i.e.* monomers, dimers, and higher order-structures. The latter are thought to correspond to enzyme oligomers, because they are prevalent only at low digitonin concentrations (35). Ultrastructural studies of intact mitochondria have demonstrated that in the native membrane the prevalent form of the enzyme is represented by oligomers, which originate from the lateral association of dimers thus generating long rows that critically contribute to the shape of the cristae (1, 10, 36, 37). We must therefore conclude that digitonin disrupts oligomers and dimers even under the mildest extraction conditions, as indicated by the presence of as many monomers as dimers/oligomers in the CN- and BN-PAGE (see for example Figs. 1–3 and Fig. S2). Coomassie dye binding to the surface of proteins contributes to further destabilize the digitonin-extracted oligomers/dimers. This means that the monomer–monomer interfaces (which are located within the inner membrane and involve subunits e and g) are based on noncovalent interactions and become labile particularly under the conditions of BN-PAGE analysis (34).

Role of eArg-8 in the stability of F-ATP synthase dimers

In this study we have identified residue Arg-8 of yeast subunit e as critical in mediating the interaction between subunits e and g. Indeed, the R8A and R8E substitutions led to decreased stability of dimeric F-ATP synthase to digitonin, with increased

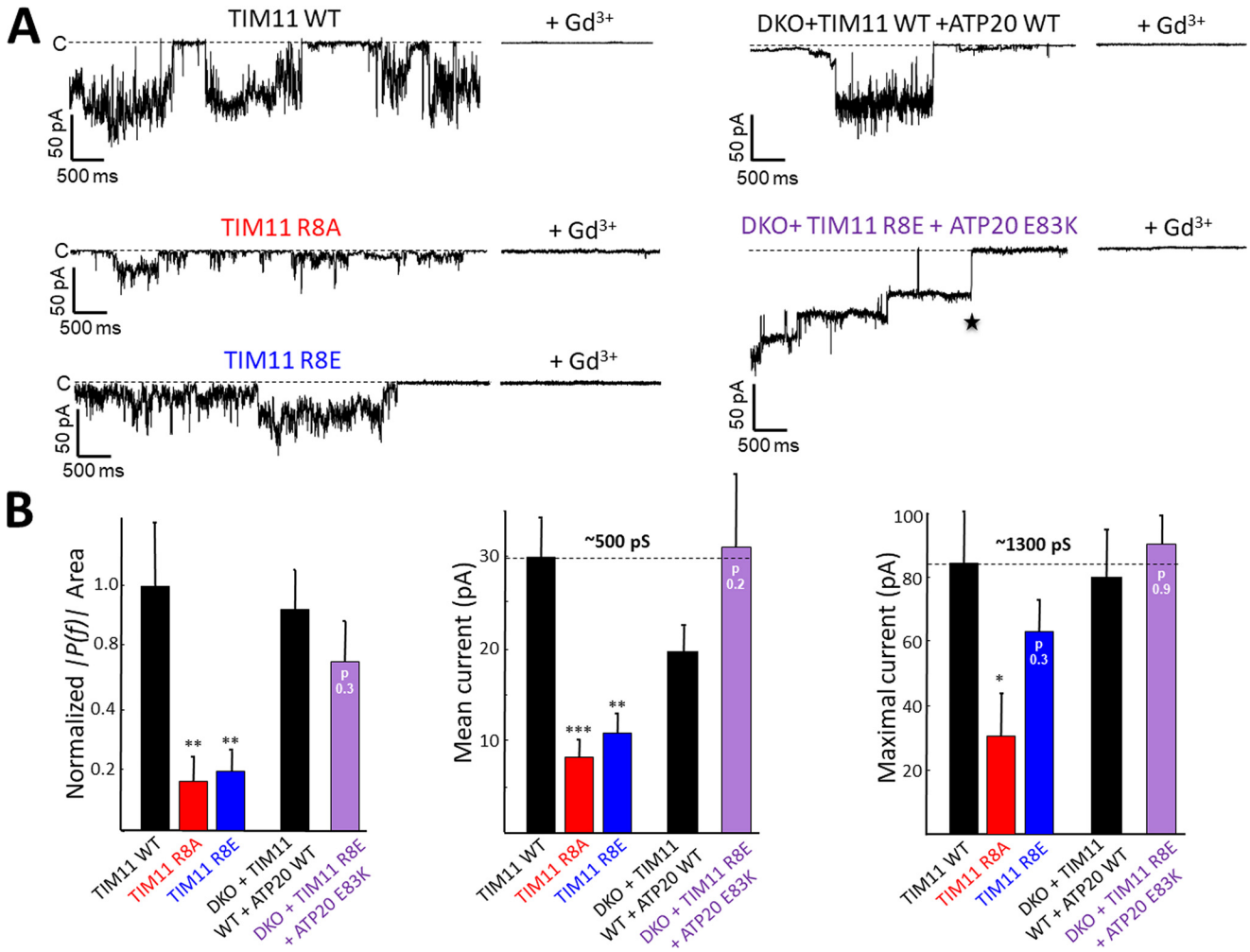

Figure 4. Electrostatic interaction between subunits e and g favors the generation of the full-conductance MMC/PTP. Mitochondria isolated from TIM11 WT, TIM11 R8A, and TIM11 R8E strains were separated by BN-PAGE after extraction with a digitonin–to–protein ratio of 0.5 g/g. Mitochondrial extracts of DKO + TIM11 WT + ATP20 WT, and DKO + TIM11 R8E + ATP20 E83K strains were subjected to BN-PAGE as described in Fig. 3*C*. Dimers were cut and eluted for planar lipid bilayers experiments. *A,* current traces elicited after insertion of purified dimeric F-ATP synthase from indicated genotypes into planar lipid bilayer following the addition of 3 mM Ca^{2+} to the *trans* side. Both *cis* and *trans* compartments already contained 100 μM PhAsO and 5 μM $Cu(OP)_2$. Channel activity was inhibited by the addition of 1 mM Gd^{3+}. $V_{cis} = -60$ mV. *Dotted lines* indicate the closed state of the channel (0 pA). The *star* in the DKO + TIM11 R8E + ATP20 E83K trace marks a single channel opening with conductance similar to that observed in the TIM11 WT. *B,* average relative $|P(f)|$ area, mean and maximal current of the indicated genotypes. Data are mean ± S.E. of 5 (TIM11 WT) or 7 (all other genotypes) independent experiments. *, $p < 0.05$ *versus* TIM11 WT; **, $p < 0.01$ *versus* TIM11 WT ; ***, $p < 0.001$ *versus* TIM11 WT. One-way ANOVA was used for statistical analysis. *p* values shown in the columns refer to the matching wildtypes (*black columns*).

appearance of monomers at detergent concentrations that usually do not disrupt dimers in BN-PAGE. A possible explanation is that an electrostatic interaction occurs between Arg-8 of subunit e and Glu-83 of subunit g, whose putative positions are shown in Fig. 6. Based on the most recent cryo-EM map of the yeast F-ATP synthase dimer, the e and g subunits contribute to form a dynamic domain responsible for bending the mitochondrial inner membrane (8). The estimated distance may appear too large for formation of a salt bridge between Arg-8 of subunit e and Glu-83 of subunit g (Fig. 6). However, the reported structure provides a static picture of the most populated state of the enzyme complex at low temperature, which may not reflect dynamic changes occurring *in situ*. For example, the distance of Cys-23 of subunit a at the dimer interface is 22 Å, yet upon treatment with copper these cysteines do form disulfide bridges at room temperature (25, 38) but not on ice (38).

It should also be considered that the side-chain details for subunits e and g in the cryo-EM are lacking, and density maps only allowed their reconstruction by polyalanine modeling, which significantly reduced the definition of this region (8). In determining the relative orientation of subunits e and g, the authors postulated that they must interact through their G*XXX*G motifs (8). The involvement of the G*XXX*G motif of subunit e in the formation of dimeric/oligomeric forms of F-ATP synthase has been well-documented, as insertion of an extra Ala or replacement of Glu with Leu led to loss of subunit g and of the enzyme supramolecular structures (29). However, the role of the G*XXX*G sequence of subunit g in enzyme dimerization is still debated, because replacement of the first Glu with Leu or Val did not affect the stability of the digitonin-extracted F-ATP synthase dimers, suggesting that this G*XXX*G motif does not act as a canonical helix–helix interaction domain (31).

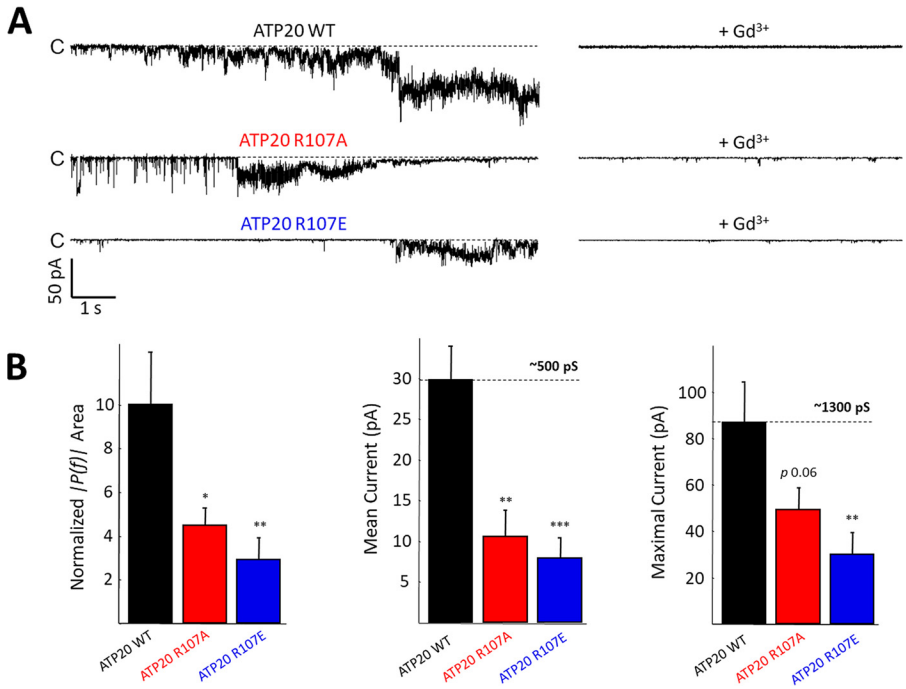

Figure 5. Mutations of gArg-107 affect the properties of MMC/PTP. Mitochondrial extracts from ATP20 WT, ATP20 R107A, and ATP20 R107E strains with a digitonin–to–protein ratio of 1.5 g/g were separated by BN-PAGE. Dimers were cut and eluted for planar lipid bilayers experiments. Experimental conditions were as described in Fig. 4. *A,* current traces elicited after insertion of purified dimeric F-ATP synthase from indicated strains into planar lipid bilayer. *B,* average relative $|P(f)|$ area, mean, and maximal current of the indicated genotypes. Data are mean ± S.E. of 5 independent experiments for ATP20 WT, 14 independent experiments for ATP20 R107A, and 9 independent experiments for ATP20 R107E. *, $p < 0.05$ *versus* ATP20 WT; **, $p < 0.01$ *versus* ATP20 WT; ***, $p < 0.001$ *versus* ATP20 WT. One-way ANOVA was used for statistical analysis.

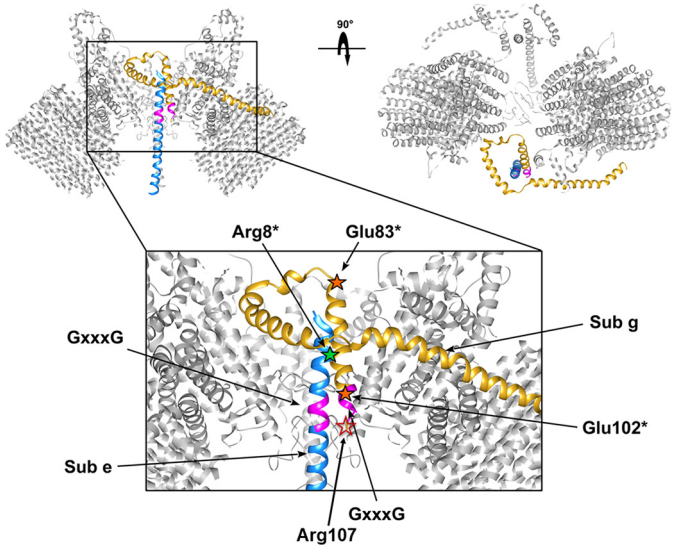

Figure 6. Overview of F-ATP synthase F_O dimer (PDB code 6B2Z). Front and top views highlight the relative position of subunits g (*yellow*) and e (*light blue*). Putative G*XXX*G dimerization motifs are marked in *purple*. *Stars* mark the positions of Arg-8 of subunit e and of Arg-107, Glu-83, and Glu-102 of subunit g.

An additional issue is that the G*XXX*G motifs have also been proposed to mediate the interaction between the two subunits e or g, thus also facilitating the lateral association of F-ATP synthase dimers into oligomers (39). Indeed, subunit e homodimers have been found exclusively in F-ATP synthase oligomers (29). Moreover, in a subunit g C75S/L109C double mutant (where the endogenous Cys residue was replaced with a Cys residue inserted very close to the G*XXX*G motif), Cu^{2+}-dependent subunit g homodimers were only found in F-ATP synthase oligomers (30). Taken together, these observations strongly suggest that e/e and g/g interactions mediated by the G*XXX*G motifs also participate in forming an F-ATP synthase oligomerization interface, which appears to be rather unstable because it is easily disrupted by digitonin (34, 39). Thus, subunits e and g, which combine membrane-surface and membrane-embedded chains, probably form flexible chains free to engage in transiently stable interactions with different target sequences, making, in turn, possible the formation of a salt bridge between Arg-8 of subunit e and Glu-83 of subunit g. Finally, the amino acid sequence of the C-terminal half of subunit e has the potential for the formation of a coiled-coil structure (40), which is typical of proteins undergoing significant conformational changes. In this sense, evidence that this coiled-coil motif may stabilize F-ATP synthase dimers–oligomers is particularly fascinating (41).

Our finding that Arg-8 of subunit e may interact with Glu-83 of subunit g in F-ATP synthase dimers suggests that other residues besides the G*XXX*G motifs (8) contribute to the e–g interface contacts, providing a further piece of information for the molecular positioning of subunits e and g within the yeast F_O sector. It is remarkable that cristae morphology, growth properties, and oxidative phosphorylation were not affected in the Arg-8 mutants; yet, an interesting phenotype was discovered by studying the channel activity of gel-purified dimer preparations.

Role of eArg-8 in channel activity of F-ATP synthase

Various studies suggest that the PTP forms from F-ATP synthase, as discussed in recent reviews (20, 42). We have suggested that the pore forms as a consequence of Ca^{2+}-dependent

conformational changes of the F_1 catalytic sites that are transmitted through the lateral stalk to the inner membrane, where subunits e and g are located in the enzyme dimers (19, 24). Genetic ablation of these subunits caused desensitization to Ca^{2+} of the PTP (22) and drastically decreased channel activity of the isolated F-ATP synthase dimers (25). Of specific relevance to a possible mechanism of pore formation are the recent findings that Arg-107 of yeast subunit g, which is located immediately after the G*XXX*G motif, specifically mediates PTP sensitivity to phenylglyoxal and that in the native enzyme solute permeation through the PTP is decreased after formation of a phenylglyoxal adduct with this residue (28). The putative position of gArg-107 is shown in Fig. 6. Based on the present results, it can be speculated that although the G*XXX*G motif plays a role in the association of subunits e and g, other residues like eArg-8 and gGlu-83 may form stable contacts allowing correct positioning of these subunits during PTP activation. Irrespective of the mechanism, however, our findings suggest that an electrostatic interaction between subunit e and subunit g in yeast F-ATP synthase dimers is essential for both dimer stability and for formation of the full-conductance MMC/PTP.

The hypothesis that the PTP forms from F-ATP synthase has been apparently questioned by genetic ablation of subunits b and OSCP of the peripheral stalk (43) and of subunit c in the F_O sector (27). However, recent electrophysiological data obtained in F-ATP synthase subunit e/g null yeast preparations (25) and in c subunit null mitoplasts (26) indicate that the high-conductance PTP is no longer present in either species (25, 26). In both cases, a residual low-conductance channel activity was detected instead (25, 26), which in mammalian cells could be inhibited by both cyclosporin A and by bongkrekate, suggesting that it may form from the adenine nucleotide translocator (26). This small channel is probably responsible for the persistent cyclosporin A–sensitive Ca^{2+} release observed by He *et al.* (27, 43) in cells null for subunits b, OSCP, and c. Thus, the proposal that the PTP forms from a specific Ca^{2+}-dependent conformation of F-ATP synthase remains fully viable (42) and is further supported by the data presented in this work.

Experimental procedures

Reagents and yeast strains

Digitonin, P_i, EGTA, sucrose, Trizma base (Tris), yeast extract, bacto-polypeptone, galactose, DTT, sorbitol, mannitol, $CaCl_2$ were from Sigma (Milan, Italy). Zymolyase 100T was purchased from US Biological. The QuikChange Lightning site-directed mutagenesis kit was purchased from Agilent Technologies. Antibodies for TIM11, ATP20, ATP4, and γ subunits were a kind gift of Dr. Marie-France Giraud, University of Bordeaux, France. The *S. cerevisiae* strains BY4743, Δ*TIM11,* and Δ*ATP20* were purchased from Thermo Fisher Scientific. Δ*TIM11*Δ*ATP20* was obtained as described previously (22).

Site-directed mutagenesis in yeast cells

The oligonucleotide primers used for TIM11 R8A, TIM11 R8E, ATP20 E83A, ATP20 E102A, and ATP20 E83K site-directed mutagenesis were as follows: TIM11 R8A (forward) CGACAGTTAATGTTTTG**GC**ATACTCTGCGTTGGGTTTG and (reverse) CAAACCCAACGCAGAGTAT**GC**CAAAACATTAACTGTCG; TIM11 R8E (forward) CGACAGTTAATGTTTTG**GA**ATACTCTGCGTTGGGTTTG and (reverse) CAAACCCAACGCAGAGTAT**TC**CAAAACATTAACTGTCG; ATP20 E83A (forward) CATCCAAAAGAATG**C**ACTATTAAAATATGGCGC and (reverse) GCGCCATATTTTAATAGT**G**CATTCTTTTGGATG; ATP20 E102A (forward) TTATTCTGTCGGTG**C**AATAATTGGAAGAAGAAA and (reverse) TTTCTTCTTCCAATTATT**G**CACCGACAGAATAA; ATP20 E83K (forward) CATCCAAAAGAAT**A**AACTATTAAAATATGGCGC and (reverse) GCGCCATATTTTAATAGTT**T**ATTCTTTTGGATG; and ATP20 E102K (forward) TTATTCTGTCGGT**A**AAATAATTGGAAGAAGAAA and (reverse) TTTCTTCTTCCAATTATTT**T**ACCGACAGAATAA. The QuikChange Lightning site-directed mutagenesis kit was used to harvest point mutations using TIM11 and ATP20 WT genes cloned in pFL38 vector as template. The mutations were checked by sequencing. One-step transformation protocol, as described previously (44), was used to transform the plasmid into Δ*TIM11* or Δ*ATP20* or Δ*TIM11*Δ*ATP20 S. cerevisiae* strains, which were plated on 2% glucose (Drop-out– uracil)-selective medium at 30 °C.

Yeast mitochondria preparation and oxygen consumption assay

Yeast strains BY4743, Δ*TIM11*, Δ*ATP20*, and Δ*TIM11*Δ*ATP20* were pre-cultured in YPG medium (1% yeast extract, 1% bacto-polypeptone, and 2% glucose) at 30 °C. TIM11 WT, TIM11 R8A, TIM11 R8E, ATP20 WT, ATP20 E83A, and ATP20 E102A mutant strains were pre-cultured in 2% glucose (Drop-out– uracil)-selective medium at 30 °C. For preparation of mitochondria, yeast cells were cultured with a starting A_{600} 0.2 in 400 ml of medium containing 1% yeast extract, 1% bacto-polypeptone, and 2% galactose overnight at 30 °C with rotation (180 rpm) and harvested in logarithmic growth phase by centrifugation at 2000 × *g* for 5 min. The cell pellet was resuspended in 0.1 M Tris-SO_4, pH 9.4 buffer, supplemented with 10 mM DTT and incubated at 37 °C for 15 min with rotation (180 rpm). The cell pellet was washed once with 1.2 M sorbitol, 20 mM P_i, pH 7.4 buffer, and incubated in the above sorbitol buffer supplemented with zymolyase 0.4 mg/g pellet at 30 °C for 45 min with rotation (180 rpm). The incubation was terminated by centrifugation at 2000 × *g* for 5 min, and the pellet was washed once with the above sorbitol buffer at 4 °C. The cell pellet was resuspended in cold isolation buffer (0.6 M mannitol, 10 mM Tris-HCl, 0.1 mM EDTA, pH 7.4) and homogenized with a Potter homogenizer. The homogenate was spun for 5 min at 2000 × *g*, and the supernatant was collected and centrifuged for 10 min at 12,000 × *g*. The mitochondrial pellet was suspended in the isolation buffer. The protein concentration was determined by measuring the absorbance at 280 nm of 0.6% SDS-solubilized mitochondria (A_{280} 0.21 corresponds to 10 mg/ml protein) (45).

A Clark-type oxygen electrode was used to detect the oxygen consumption of isolated yeast mitochondria. A half mg of mitochondria was incubated in 250 mM sucrose, 10 mM Tris-MOPS, 30 μM EGTA, 10 mM P_i, 0.5 mg/ml BSA, pH 7.4, in a final volume of 2 ml. 1 mM NADH, 0.2 mM ADP, 4 μM oligomycin,

and 1 μM carbonylcyanide-*p*-(trifluoromethoxy)phenylhydrazone (FCCP) were added sequentially.

Yeast cell lysis and Western blotting

Yeast strains were cultured in YPG medium or 2% glucose (Drop-out–uracil) selective medium (as mentioned above) overnight at 30 °C. About 5×10^7 cells ($A_{600\,nm}$ of 3) were harvested and washed once with 1 ml of cold H_2O. Cell pellet was resuspended in 0.1 M NaOH and incubated at 25 °C for 10 min. The incubation was terminated by centrifugation, and the resulting pellet was solubilized in 50 μl of SDS-PAGE loading buffer (50 mM Tris-HCl, pH 6.8, 20% v/v glycerol, 5% v/v β-mercaptoethanol, 2% w/v SDS, and 0.04% w/v bromphenol blue). The sample was heated at 95 °C for 3 min, followed by centrifugation at 12,000 $\times$ *g* for 10 min at 4 °C, and 25 μl of the lysates was subjected to SDS-PAGE. Isolated mitochondria were lysed in the above SDS-PAGE loading buffer at a concentration of 5 μg/μl and heated at 95 °C for 3 min. Lysates (10 μl) were loaded onto NuPAGE™ 12% BisTris Protein Gels (Invitrogen), and proteins were separated by electrophoresis in MOPS SDS Running Buffer (Invitrogen) for 3 h at 20 mA at 4 °C. Proteins were transferred onto nitrocellulose membranes at 30 V for 1.25 h at 4 °C. The membrane was blocked with 5% (w/v) milk at room temperature for 1 h and incubated with the antibodies against *TIM11*, *ATP20*, *ATP4*, and γ subunits overnight at 4 °C. Immunoreactive bands were detected by chemiluminescence using an Uvitec Cambridge instrument.

Cross-linking experiments

Isolated yeast mitochondria were suspended at a protein concentration of 1 mg $\times$ ml^{-1} in 250 mM sucrose, 10 mM Tris-MOPS, 2 mM P_i, 10 μM EGTA, pH 7.4. The cross-linking reaction was carried out with the addition of 2 mM $CuCl_2$ and incubation at room temperature for 15 min. The reaction was stopped with the addition of 5 mM EDTA and 5 mM *N*-ethylmaleimide followed by incubation on ice for 10 min. Mitochondrial pellet was collected by centrifugation at 12,000 $\times$ *g* for 10 min at 4 °C and subjected to the BN-PAGE analyses.

Blue and clear native-gel electrophoresis

Yeast mitochondria were suspended at a protein concentration of 10 mg $\times$ ml^{-1} in 150 mM potassium acetate, 30 mM HEPES, 10% v/v glycerol, 1 mM phenylmethylsulfonyl fluoride, pH 7.4, and supplemented with the amounts of digitonin indicated in the figure legends. The mitochondrial lysates were centrifuged at 100,000 $\times$ *g* for 25 min at 4 °C with a Beckman TL-100 rotor. The supernatants were supplemented with 50 mM BisTris, 50 mM NaCl, 10% w/v glycerol, 0.001% Ponceau S, pH 7.4, with HCl for CN-PAGE (35) or with native PAGE 5% G-250 sample additive (Invitrogen) for BN-PAGE and loaded onto NativePAGE™ 3–12% gradient BisTris protein gels (BN-PAGE, Invitrogen) (10 μl/well). CN-PAGE was carried out at 4 °C using 50 mM BisTris, 50 mM Tricine, pH 6.8. Electrophoresis was initiated at 100 V for about 15 min to allow the samples to enter the gels. The voltage was then increased to 300 V, and the electrophoresis was stopped after about 2 h. BN-PAGE was carried out in the Dark Blue cathode buffer at 150 V for 20 min and in the Light Blue cathode buffer at 250 V for 2 h. After electrophoresis, BN gels were stained with 0.25 mg/ml Coomassie Blue, 10% acetic acid at room temperature overnight, or with in-gel activity staining for ATP hydrolysis. CN gels were only stained with in-gel activity staining. Activity was monitored in 270 mM glycine, 35 mM Tris, pH 7.4, 8 mM ATP-Tris, pH 7.4, 15 mM $MgSO_4$, and 2 mg/ml $Pb(NO_3)_2$ at 37 °C. For Western blot analysis, CN or BN gels were blotted PVDF membranes. F-ATP synthase bands were excised and treated as described below.

Electrophysiology

Excised dimers of F-ATP synthase from BN-polyacrylamide gels were eluted with 25 mM Tricine, 7.5 mM BisTris, pH 7.0, supplemented with 8 mM ATP-Tris, pH 7.4, 10 mM $MgSO_4$, and 1% w/v *n*-heptyl β-D-thioglucopyranoside with rotation overnight at 4 °C. The eluate was centrifuged at 20,000 $\times$ *g* for 20 min at 4 °C, and the supernatants were collected for reconstitution in electrophysiological analyses. Electrophysiological properties of F-ATP synthase were assessed by means of multisite single channel recording following protein insertion into artificial planar lipid bilayers. Multiple electrophysiological recordings were assessed at the same time from the same sample with an Orbit mini bilayer work station (Nanion Technologies, Munich, Germany) enabling the simultaneous recording of up to four artificial lipid bilayers. Membranes were prepared by painting a solution (10 mg/ml in octane) of soybean asolectin (Sigma) across four microcavities (150 μm in diameter) on standard Multielectrode Cavity Array (Meca) 4 chips (IonEra, Freiburg, Germany), set on the bottom of the Orbit mini recording chamber. Prior to membrane painting, the whole recording chambers were filled with a recording solution (150 mM KCl, 10 mM HEPES, pH 7.4, 100 μM PhAsO, and 5 μM $Cu(OP)_2$). The microcavities of the chip constituted the *cis* compartment, to which all reported voltages refer, with zero being assigned by convention to the *trans* (grounded) side. Currents were considered as positive when carried by cations flowing from the *cis* to the *trans* compartment, and vice versa. Currents were elicited with the addition of 3 mM $CaCl_2$ to the *trans* compartment after the protein had been loaded into the recording chambers. Membrane capacity ranged from 10 to 80 pF (average 50 pF), and no current leakage was detectable. Control recordings from empty membrane showed no current occurrence during the whole recording time of up to 30 min. Data were acquired at 5 KHz, filtered at 500 Hz using a low-pass 4-pole Bessel filter, digitalized, and stored on a computer by a dedicated software (EDR, Elements s.r.l, Italy). Data were analyzed offline using MATLAB 2007b (MathWorks). The power spectrum for each current signal was calculated by means of the Fast Fourier transform; frequencies lower than 5 Hz (baseline drifts) and higher than 500 Hz were not included in the analysis. The area under the power spectrum curve, referred for brevity as $|P(f)|$, as well as mean currents for nonzero values, and maximal currents were calculated for each condition, taking advantage of a homemade algorithm developed on MATLAB. Averaged $|P(f)|$ values were normalized for the WT value. Data are represented as mean $\pm$ S.E. Statistical comparison of data were assessed with ANOVA analysis.

Author contributions—L. G., M. C., G. M., I. M., P. B., and G. L. conceptualization; L. G., A. C., and A. U. data curation; L. G., G. M., A. U., and S. C. T. formal analysis; L. G. and A. C. investigation; L. G. and M. C. methodology; L. G., A. C., P. B., and G. L. writing-original draft; L. G., I. S., P. B., and G. L. writing-review and editing; M. C., I. S., P. B., and G. L. supervision; G. M. visualization; S. C. T. and P. B. funding acquisition; P. B. project administration.

Acknowledgments—We thank Dr. Marco Ardina for assistance with informatics, and we thank the EM facility of the Dept. of Biology, University of Padova. We are grateful to Dr. Ming-Hong He and Dr. Jin-Qiu Zhou of Shanghai Institute of Biochemistry and Cell Biology, Chinese Academy of Sciences, for their kind help with the yeast growth experiment.

References

1. Kühlbrandt, W. (2019) Structure and mechanisms of F-type ATP synthases. *Annu. Rev. Biochem.* **88,** 2019 CrossRef Medline
2. Walker, J. E., Fearnley, I. M., Gay, N. J., Gibson, B. W., Northrop, F. D., Powell, S. J., Runswick, M. J., Saraste, M., and Tybulewicz, V. L. (1985) Primary structure and subunit stoichiometry of F_1-ATPase from bovine mitochondria. *J. Mol. Biol.* **184,** 677–701 CrossRef Medline
3. Abrahams, J. P., Leslie, A. G., Lutter, R., and Walker, J. E. (1994) Structure at 2.8 Å resolution of F_1-ATPase from bovine heart mitochondria. *Nature* **370,** 621–628 CrossRef Medline
4. Lau, W. C., Baker, L. A., and Rubinstein, J. L. (2008) Cryo-EM structure of the yeast ATP synthase. *J. Mol. Biol.* **382,** 1256–1264 CrossRef Medline
5. Klusch, N., Murphy, B. J., Mills, D. J., Yildiz Ö., and Kühlbrandt W. (2017) Structural basis of proton translocation and force generation in mitochondrial ATP synthase. *Elife* **6,** e33274 CrossRef Medline
6. Hahn, A., Parey, K., Bublitz, M., Mills, D. J., Zickermann, V., Vonck, J., Kühlbrandt, W., and Meier, T. (2016) Structure of a complete ATP synthase dimer reveals the molecular basis of inner mitochondrial membrane morphology. *Mol. Cell* **63,** 445–456 CrossRef Medline
7. Srivastava, A. P., Luo, M., Zhou, W., Symersky, J., Bai, D., Chambers, M. G., Faraldo-Gómez, J. D., Liao, M., and Mueller, D. M. (2018) High-resolution cryo-EM analysis of the yeast ATP synthase in a lipid membrane. *Science* **360,** eaas9699 CrossRef Medline
8. Guo, H., Bueler, S. A., and Rubinstein, J. L. (2017) Atomic model for the dimeric F_O region of mitochondrial ATP synthase. *Science* **358,** 936–940 CrossRef Medline
9. Anselmi, C., Davies, K. M., and Faraldo-Gómez, J. D. (2018) Mitochondrial ATP synthase dimers spontaneously associate due to a long-range membrane-induced force. *J. Gen. Physiol.* **150,** 763–770 CrossRef Medline
10. Davies, K. M., Anselmi, C., Wittig, I., Faraldo-Gómez, J. D., and Kühlbrandt, W. (2012) Structure of the yeast F1Fo-ATP synthase dimer and its role in shaping the mitochondrial cristae. *Proc. Natl. Acad. Sci. U.S.A.* **109,** 13602–13607 CrossRef Medline
11. Strauss, M., Hofhaus, G., Schröder, R. R., and Kühlbrandt, W. (2008) Dimer ribbons of ATP synthase shape the inner mitochondrial membrane. *EMBO J.* **27,** 1154–1160 CrossRef Medline
12. Arnold, I., Pfeiffer, K., Neupert, W., Stuart, R. A., and Schägger, H. (1998) Yeast mitochondrial F_1F_0-ATP synthase exists as a dimer: identification of three dimer-specific subunits. *EMBO J.* **17,** 7170–7178 CrossRef Medline
13. Paumard, P., Vaillier, J., Coulary, B., Schaeffer, J., Soubannier, V., Mueller, D. M., Brèthes, D., di Rago, J. P., and Velours, J. (2002) The ATP synthase is involved in generating mitochondrial cristae morphology. *EMBO J.* **21,** 221–230 CrossRef Medline
14. Arselin, G., Vaillier, J., Salin, B., Schaeffer, J., Giraud, M. F., Dautant, A., Brèthes, D., and Velours, J. (2004) The modulation in subunits e and g amounts of yeast ATP synthase modifies mitochondrial cristae morphology. *J. Biol. Chem.* **279,** 40392–40399 CrossRef Medline
15. Soubannier, V., Vaillier, J., Paumard, P., Coulary, B., Schaeffer, J., and Velours, J. (2002) In the absence of the first membrane-spanning segment of subunit 4(b), the yeast ATP synthase is functional but does not dimerize or oligomerize. *J. Biol. Chem.* **277,** 10739–10745 CrossRef Medline
16. Soubannier, V., Rusconi, F., Vaillier, J., Arselin, G., Chaignepain, S., Graves, P. V., Schmitter, J. M., Zhang, J. L., Mueller, D., and Velours, J. (1999) The second stalk of the yeast ATP synthase complex: identification of subunits showing cross-links with known positions of subunit 4 (subunit b). *Biochemistry* **38,** 15017–15024 CrossRef Medline
17. Giorgio, V., von Stockum, S., Antoniel, M., Fabbro, A., Fogolari, F., Forte, M., Glick, G. D., Petronilli, V., Zoratti, M., Szabó, I., Lippe, G., and Bernardi, P. (2013) Dimers of mitochondrial ATP synthase form the permeability transition pore. *Proc. Natl. Acad. Sci. U.S.A.* **110,** 5887–5892 CrossRef Medline
18. Bernardi, P., Rasola, A., Forte, M., and Lippe, G. (2015) The mitochondrial permeability transition pore: channel formation by F-ATP synthase, integration in signal transduction, and role in pathophysiology. *Physiol. Rev.* **95,** 1111–1155 CrossRef Medline
19. Giorgio, V., Guo, L., Bassot, C., Petronilli, V., and Bernardi, P. (2018) Calcium and regulation of the mitochondrial permeability transition. *Cell Calcium* **70,** 56–63 Medline
20. Bernardi, P., and Lippe, G. (2018) Channel formation by F-ATP synthase and the permeability transition pore: an update. *Curr. Opin. Physiol.* **3,** 1–5 CrossRef
21. Alavian, K. N., Beutner, G., Lazrove, E., Sacchetti, S., Park, H. A., Licznerski, P., Li, H., Nabili, P., Hockensmith, K., Graham, M., Porter, G. A., Jr., and Jonas, E. A. (2014) An uncoupling channel within the c-subunit ring of the F_1F_O ATP synthase is the mitochondrial permeability transition pore. *Proc. Natl. Acad. Sci. U.S.A.* **111,** 10580–10585 CrossRef Medline
22. Carraro, M., Giorgio, V., Šileikytė, J., Sartori, G., Forte, M., Lippe, G., Zoratti, M., Szabò, I., and Bernardi, P. (2014) Channel formation by yeast F-ATP synthase and the role of dimerization in the mitochondrial permeability transition. *J. Biol. Chem.* **289,** 15980–15985 CrossRef Medline
23. von Stockum, S., Giorgio, V., Trevisan, E., Lippe, G., Glick, G. D., Forte, M. A., Da-Rè, C., Checchetto, V., Mazzotta, G., Costa, R., Szabò, I., and Bernardi, P. (2015) F-ATPase of *Drosophila melanogaster* forms 53-picosiemen (53-pS) channels responsible for mitochondrial Ca^{2+}-induced Ca^{2+} release. *J. Biol. Chem.* **290,** 4537–4544 CrossRef Medline
24. Giorgio, V., Burchell, V., Schiavone, M., Bassot, C., Minervini, G., Petronilli, V., Argenton, F., Forte, M., Tosatto, S., Lippe, G., and Bernardi, P. (2017) Ca^{2+} binding to F-ATP synthase β subunit triggers the mitochondrial permeability transition. *EMBO Rep.* **18,** 1065–1076 CrossRef Medline
25. Carraro, M., Checchetto, V., Sartori, G., Kucharczyk, R., di Rago, J. P., Minervini, G., Franchin, C., Arrigoni, G., Giorgio, V., Petronilli, V., Tosatto, S. C. E., Lippe, G., Szabó, I., and Bernardi, P. (2018) High-conductance channel formation in yeast mitochondria is mediated by F-ATP synthase e and g subunits. *Cell. Physiol. Biochem.* **50,** 1840–1855 CrossRef Medline
26. Neginskaya, M. A., Solesio, M. E., Berezhnaya, E. V., Amodeo, G. F., Mnatsakanyan, N., Jonas, E. A., and Pavlov, E. V. (2019) ATP synthase C-subunit–deficient mitochondria have a small cyclosporine A-sensitive channel, but lack the permeability transition pore. *Cell Rep.* **26,** 11–17.e2 CrossRef Medline
27. He, J., Ford, H. C., Carroll, J., Ding, S., Fearnley, I. M., and Walker, J. E. (2017) Persistence of the mitochondrial permeability transition in the absence of subunit c of human ATP synthase. *Proc. Natl. Acad. Sci. U.S.A.* **114,** 3409–3414 CrossRef Medline
28. Guo, L., Carraro, M., Sartori, G., Minervini, G., Eriksson, O., Petronilli, V., and Bernardi, P. (2018) Arginine 107 of yeast ATP synthase subunit g mediates sensitivity of the mitochondrial permeability transition to phenylglyoxal. *J. Biol. Chem.* **293,** 14632–14645 CrossRef Medline
29. Arselin, G., Giraud, M. F., Dautant, A., Vaillier, J., Brèthes, D., Coulary-Salin, B., Schaeffer, J., and Velours, J. (2003) The GxxxG motif of the transmembrane domain of subunit e is involved in the dimerization/oligomerization of the yeast ATP synthase complex in the mitochondrial membrane. *Eur. J. Biochem.* **270,** 1875–1884 CrossRef Medline
30. Bustos, D. M., and Velours, J. (2005) The modification of the conserved *GXXXG* motif of the membrane-spanning segment of subunit g destabi-

lizes the supramolecular species of yeast ATP synthase. *J. Biol. Chem.* **280,** 29004–29010 CrossRef Medline

31. Saddar, S., and Stuart, R. A. (2005) The yeast F_1F_0-ATP synthase: analysis of the molecular organization of subunit g and the importance of a conserved G*XXX*G motif. *J. Biol. Chem.* **280,** 24435–24442 CrossRef Medline
32. Wittig, I., and Schägger, H. (2005) Advantages and limitations of clear-native PAGE. *Proteomics* **5,** 4338–4346 CrossRef Medline
33. Wittig, I., Karas, M., and Schägger, H. (2007) High-resolution clear native electrophoresis for in-gel functional assays and fluorescence studies of membrane protein complexes. *Mol. Cell. Proteomics* **6,** 1215–1225 CrossRef Medline
34. Wittig, I., Velours, J., Stuart, R., and Schägger, H. (2008) Characterization of domain interfaces in monomeric and dimeric ATP synthase. *Mol. Cell. Proteomics* **7,** 995–1004 CrossRef Medline
35. Wittig, I., Braun, H. P., and Schägger, H. (2006) Blue native PAGE. *Nat. Protoc.* **1,** 418–428 CrossRef Medline
36. Allen, R. D., Schroeder, C. C., and Fok, A. K. (1989) An investigation of mitochondrial inner membranes by rapid-freeze deep-etch techniques. *J. Cell Biol.* **108,** 2233–2240 CrossRef Medline
37. Dudkina, N. V., Sunderhaus, S., Braun, H. P., and Boekema, E. J. (2006) Characterization of dimeric ATP synthase and cristae membrane ultrastructure from *Saccharomyces* and *Polytomella* mitochondria. *FEBS Lett.* **580,** 3427–3432 CrossRef Medline
38. Velours, J., Stines-Chaumeil, C., Habersetzer, J., Chaignepain, S., Dautant, A., and Brèthes, D. (2011) Evidence of the proximity of ATP synthase subunits 6 (a) in the inner mitochondrial membrane and in the supramolecular forms of *Saccharomyces cerevisiae* ATP synthase. *J. Biol. Chem.* **286,** 35477–35484 CrossRef Medline
39. Habersetzer, J., Ziani, W., Larrieu, I., Stines-Chaumeil, C., Giraud, M. F., Brèthes, D., Dautant, A., and Paumard, P. (2013) ATP synthase oligomerization: from the enzyme models to the mitochondrial morphology. *Int. J. Biochem. Cell Biol.* **45,** 99–105 CrossRef Medline
40. Arnold, I., Bauer, M. F., Brunner, M., Neupert, W., and Stuart, R. A. (1997) Yeast mitochondrial F_1F_0-ATPase: the novel subunit e is identical to Tim11. *FEBS Lett.* **411,** 195–200 CrossRef Medline
41. Everard-Gigot, V., Dunn, C. D., Dolan, B. M., Brunner, S., Jensen, R. E., and Stuart, R. A. (2005) Functional analysis of subunit e of the F_1F_O-ATP synthase of the yeast *Saccharomyces cerevisiae*: importance of the N-terminal membrane anchor region. *Eukaryot. Cell* **4,** 346–355 CrossRef Medline
42. Bernardi, P. (2018) Why F-ATP synthase remains a strong candidate as the mitochondrial permeability transition pore. *Front. Physiol.* **9,** 1543 CrossRef Medline
43. He, J., Carroll, J., Ding, S., Fearnley, I. M., and Walker, J. E. (2017) Permeability transition in human mitochondria persists in the absence of peripheral stalk subunits of ATP synthase. *Proc. Natl. Acad. Sci. U.S.A.* **114,** 9086–9091 CrossRef Medline
44. Chen, D. C., Yang, B. C., and Kuo, T. T. (1992) One-step transformation of yeast in stationary phase. *Curr. Genet.* **21,** 83–84 CrossRef Medline
45. Bradshaw, P. C., and Pfeiffer, D. R. (2013) Characterization of the respiration-induced yeast mitochondrial permeability transition pore. *Yeast* **30,** 471–483 CrossRef Medline